Beam Beam Effects at the TESLA Linear Collider

O. Napoly* and D. Schulte‡
* *CEA/Saclay* ‡ *CERN, Geneva*

February 27, 2001

Abstract

The main characteristics of the beam-beam effect and its consequences on the spent beam, the beamstrahlung photon flux and the detector background are calculated for the TESLA parameters at 500 GeV and 800 GeV centre of mass energy. The issue of the beam-beam stability related to the high vertical disruption parameter is also investigated.

1 Colliding Beam Parameters and Luminosity Optimization

1.1 Flat beam parameter

Thse beam-beam interaction is very intense at the collision point of any linear collider. To minimize its effect, flat beams with large aspect ratio $R = \sigma_x^*/\sigma_y^*$ are used at the interaction point (IP). This is reflected in the current set of TESLA parameters for the beams arriving at collision (see Table 1). The large aspect ratio results in a strong beam disruption in the vertical plane. It is quantified by the disruption parameter D_y defined as the ratio of the bunch length σ_z to the vertical beam-beam focal length f_y, and given by

$$D_y \equiv \frac{\sigma_z}{f_y} = \frac{2\, r_e\, N_b\, \sigma_z}{\gamma\, \sigma_x^*(\sigma_x^* + \sigma_y^*)}$$

where N_b is the bunch population. As given by Table 1, the disruption parameter is about 25 which indicates that, in a stable e^+e^- collision regime, the particles undergo several vertical oscillations while crossing the opposite bunch.

1.2 Luminosity enhancement

Beam-beam simulations with GUINEA-PIG [1] indicate that the luminosity is a factor 2 larger than the geometric Gaussian luminosity, as a result of the mutual pinching of the e^+ and e^- bunches. As shown by Fig.1(top,left), the luminosity is maximum when the bunches are focused

Center of mass energy	[GeV]	$\sqrt{s} = 2E_0$	500	800
Luminosity	$[10^{34}\mathrm{cm}^{-2}\mathrm{s}^{-1}]$	$\mathcal{L}$	3.4	5.8
Luminosity per bunch crossing	$[10^{30}\ \mathrm{cm}^{-2}]$	$\overline{\mathcal{L}}$	2.4	3.0
Bunch population	$[10^{10}]$	N_b	2	1.4
Transverse bunch sizes	[nm]	σ_x^*, σ_y^*	553 , 5	391 , 2.8
Transverse bunch divergences	[μrad]	Θ_x^*, Θ_y^*	37 , 12	26 , 7
Normalized emittances	[mm.mrad]	$\gamma\epsilon_x$, $\gamma\epsilon_y$	10 , 0.030	8 , 0.015
Geometric emittances	[μm.μrad]	ϵ_x, ϵ_y	20 , 0.061	10 , 0.019
Beta functions	[mm]	β_x^*, β_y^*	15 , 0.4	15 , 0.4
Bunch length	[μm]	σ_z	300	300
Disruption parameters		D_x, D_y	0.22 , 25	0.20 , 27

Table 1: Parameters of the incoming beams at the IP.

Center of mass energy [GeV]	$\sqrt{s} = 2E_0$	500	800
Transverse bunch divergences [μrad]	Θ_x^D, Θ_y^D	246 , 23	150 , 17
RMS emittances [μm.μrad]	ϵ_x, ϵ_y	67 , 0.18	29 , 0.068
Beta functions [mm]	β_x, β_y	4.5 , 0.37	5.2 , 0.33
Alpha functions	α_x, α_y	1.7 , 0.68	1.7 , 0.57
Relative energy loss [%]	$\langle dE \rangle / E_0$	3.2	4.3
Relative RMS energy spread [GeV]	σ_E	13	28

Table 2: Spent beam parameters for head-on collisions. The Twiss parameters β and α are calculated at the IP position.

to vertical waists located about $0.63 \times \beta_y^* \simeq 250\,\mu$m in front of the IP ($\alpha_y^* = -0.63$ at the IP). The two other linear optics parameters which can mismatch the vertical IP beam size and affect the luminosity, namely the vertical dispersion and the xy-coupling, are shown on Fig.1(left) to be optimized when at zero (see also Ref.[2]). The right side of Fig.1 show that these optimums can be accurately reached by counting the e^+e^- pairs impinging a luminosity monitor (LUMON). This is discussed in more details in Section 3.

At 800 GeV c.m. energy, the optimization is very similar and the optimum waist w_y is found at the same position

2 Spent Beam Parameters for Head-on Collisions

During collisions the beam particles experience strong deflections and lose energy by emitting beamstrahlung photons. Therefore the transverse emittances and energy distribution of the outgoing beams are degraded compared to the incoming ones. The resulting average parameters calculated from the beam distributions assuming perfect head-on collisions (zero relative offset and angle) are given in Table 2. Compared with Table 1, the transverse emittances blow up by about a factor 3 in both planes for both c.m. energies. The transverse phase space distributions for TESLA 500 GeV are plotted in Ref.[3]. The angular and energy distributions are shown in Figs.2-4 for 500 GeV c.m. energy and in Figs.5-7 for 800 GeV c.m. energy.

The luminosity enhancement discussed in Sect.1.2 is compensated by the dilution of the luminosity spectrum $d\mathcal{L}/d\sqrt{s}$ towards lower centre of mass energies, concomitant with the energy degradation of the beam particles due to beamstrahlung photon emission. Still, as shown by Fig.8, about 60% of the total luminosity is produced at energies higher than 99.5% of the nominal c.m. energy.

3 Beam-Beam Backgrounds

3.1 Background sources

Beamstrahlung, i.e. emission of synchrotron radiation in the coherent e.m. field of the opposite bunch, is considerable at these high beam energies. It is usually characterized by the *Upsilon* parameter given by

$$\Upsilon \equiv \frac{2}{3}\frac{\langle E_c \rangle}{E_0} = \frac{5\, r_e^2\, \gamma\, N_b}{6\alpha_e \sigma_z\, (\sigma_x^* + \sigma_y^*)}$$

where $\langle E_c \rangle$ is the average photon critical energy and E_0 is the beam energy. With a photon yield of about 1.6 per electron, beamstrahlung degrades the spent beam energy distribution, with a 3-4% average energy loss, and the luminosity spectrum $d\mathcal{L}/d\sqrt{s}$, as discussed in the preceding section. A small fraction of the beamstrahlung photons are converted into low energy e^+e^-pairs which form the most numerous background source to the detector.

The main characteristics of the beam-beam background are given in Table 3. The charged particle background whose energy spectrum is plotted in Fig.9 for 500 GeV c.m. energy, is essentially the result of three basic processes :

1. beamstrahlung emission : the energy-degraded spent beam dominates the spectrum of charged particles above 100 GeV. It is discussed in Section 2. The extraction of the electron and

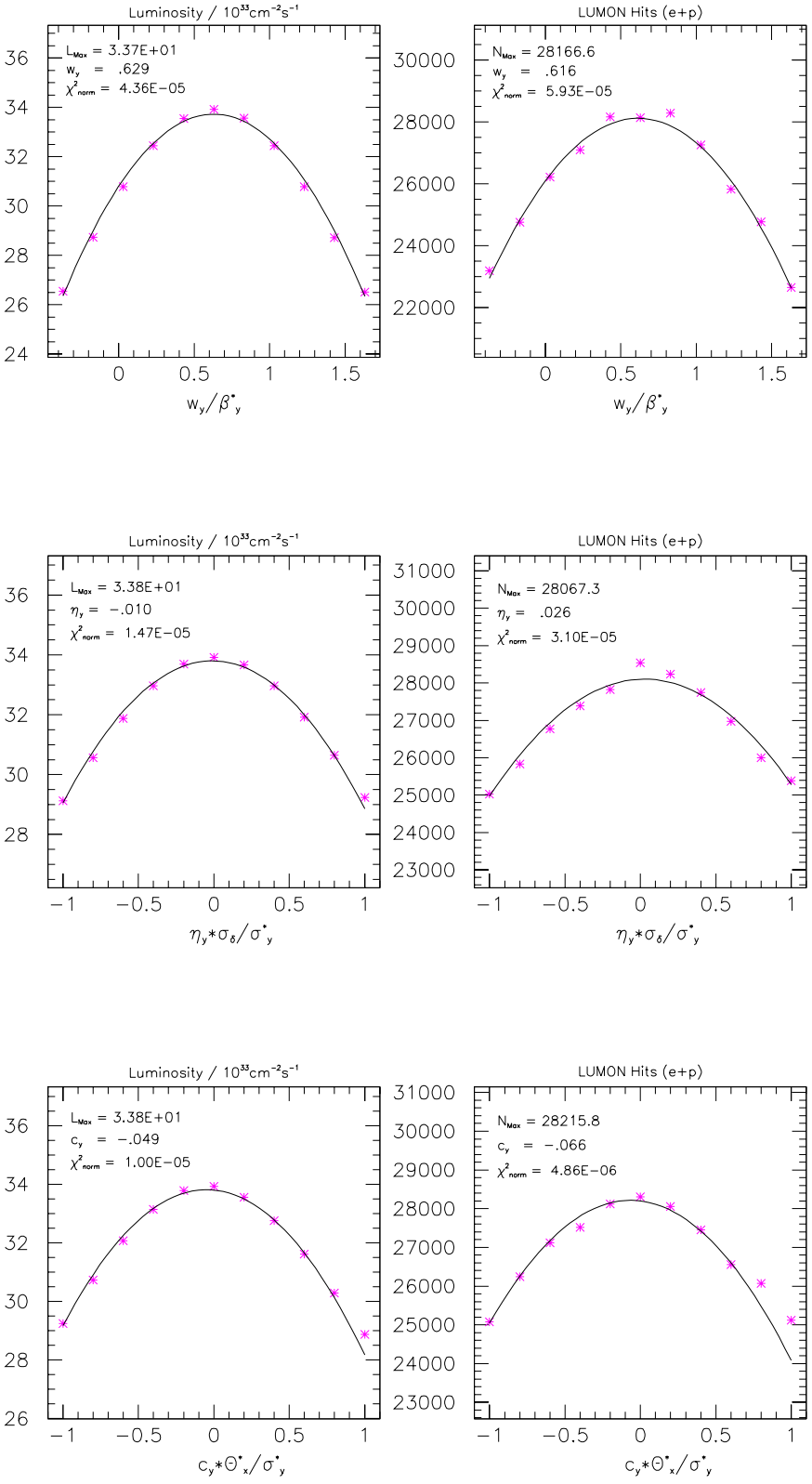

Figure 1: Luminosity optimization relative to vertical waist position w_y (top), vertical dispersion η_y (middle) and coupling c_y (bottom) [2] for TESLA 500 GeV c.m. energy. Solid lines show the parabolic fits through the 11 data points.

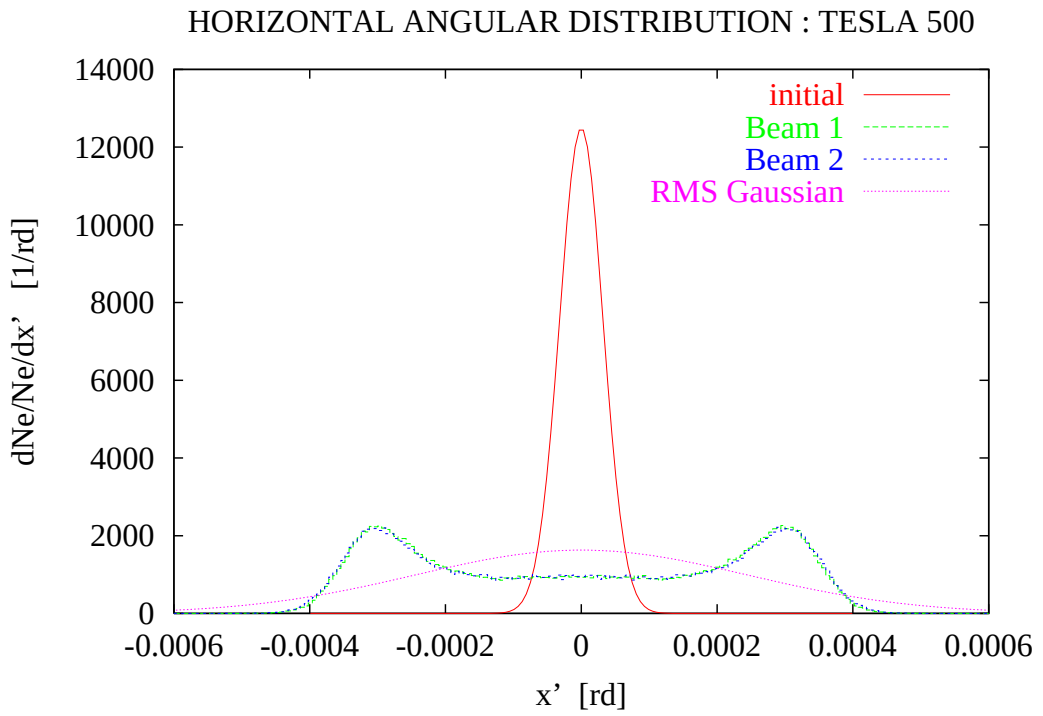

Figure 2: Spent beam angular distribution in the horizontal plane for 500 GeV c.m. energy.

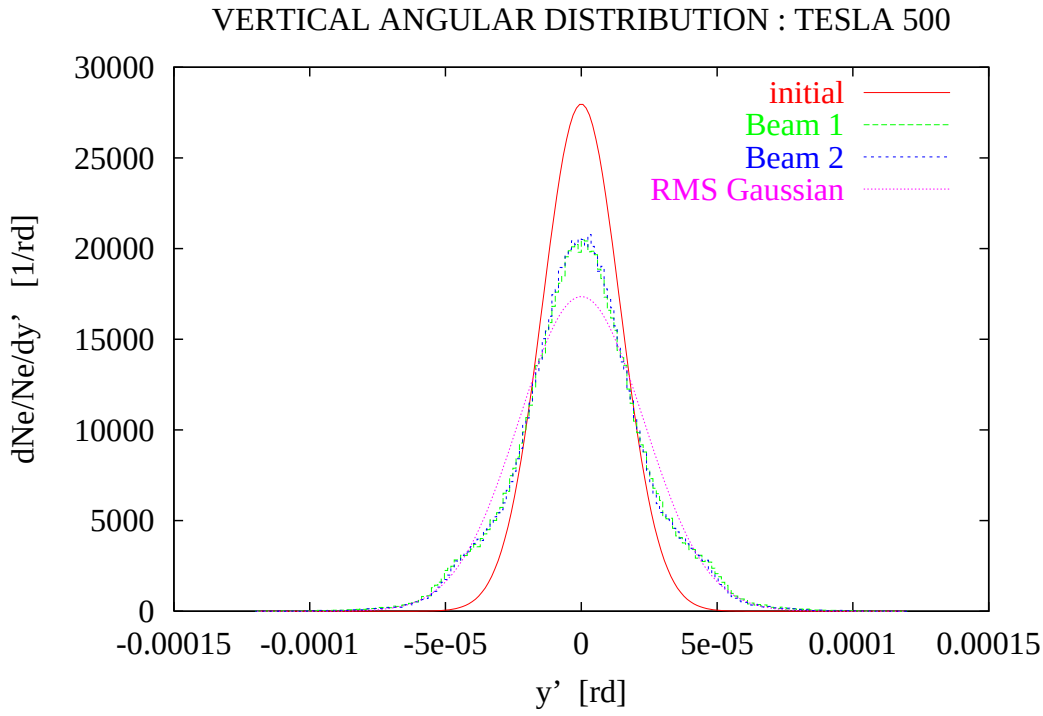

Figure 3: Spent beam angular distribution in the vertical plane for 500 GeV c.m. energy.

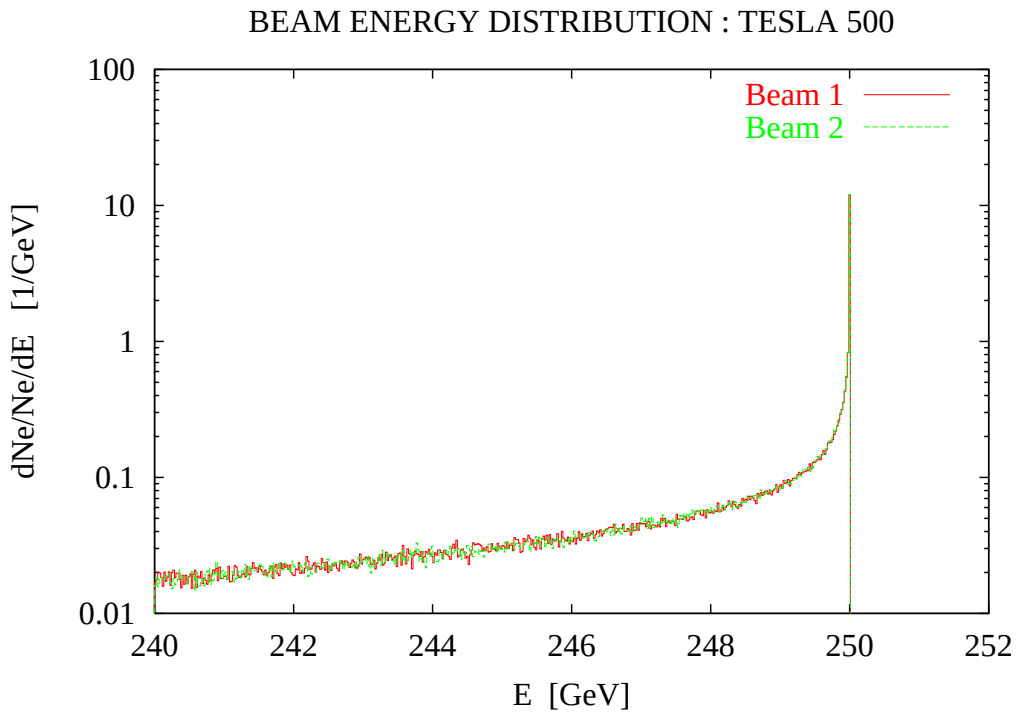

Figure 4: Spent beam energy distribution for 500 GeV c.m. energy.

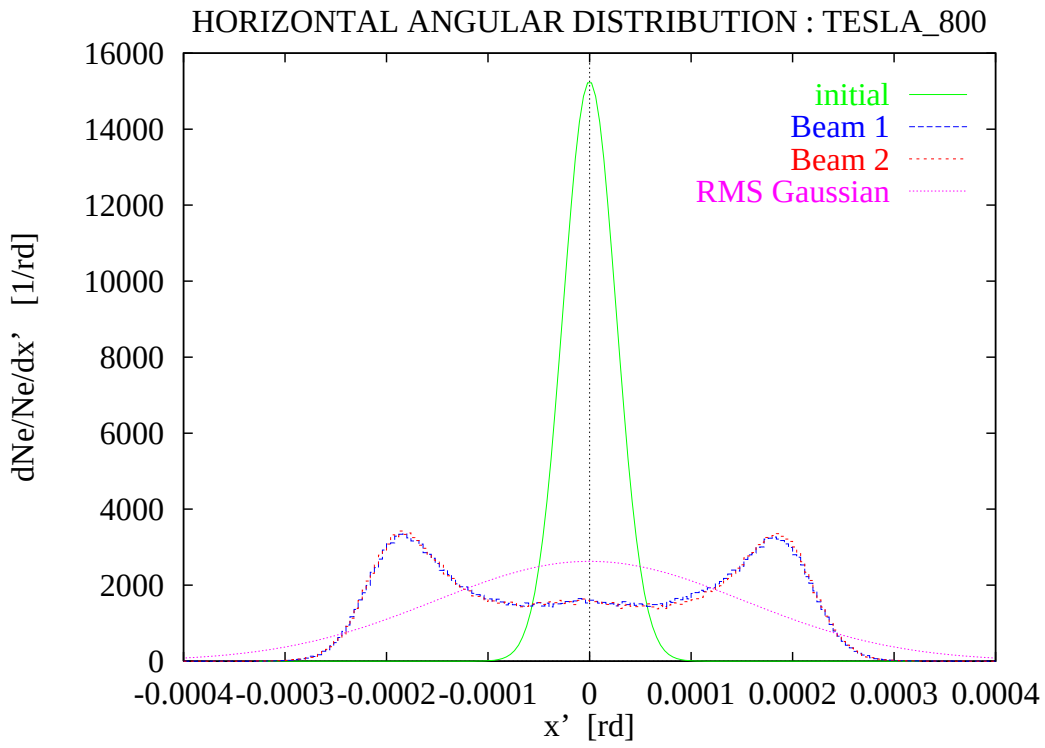

Figure 5: Spent beam angular distribution in the horizontal plane for 800 GeV c.m. energy.

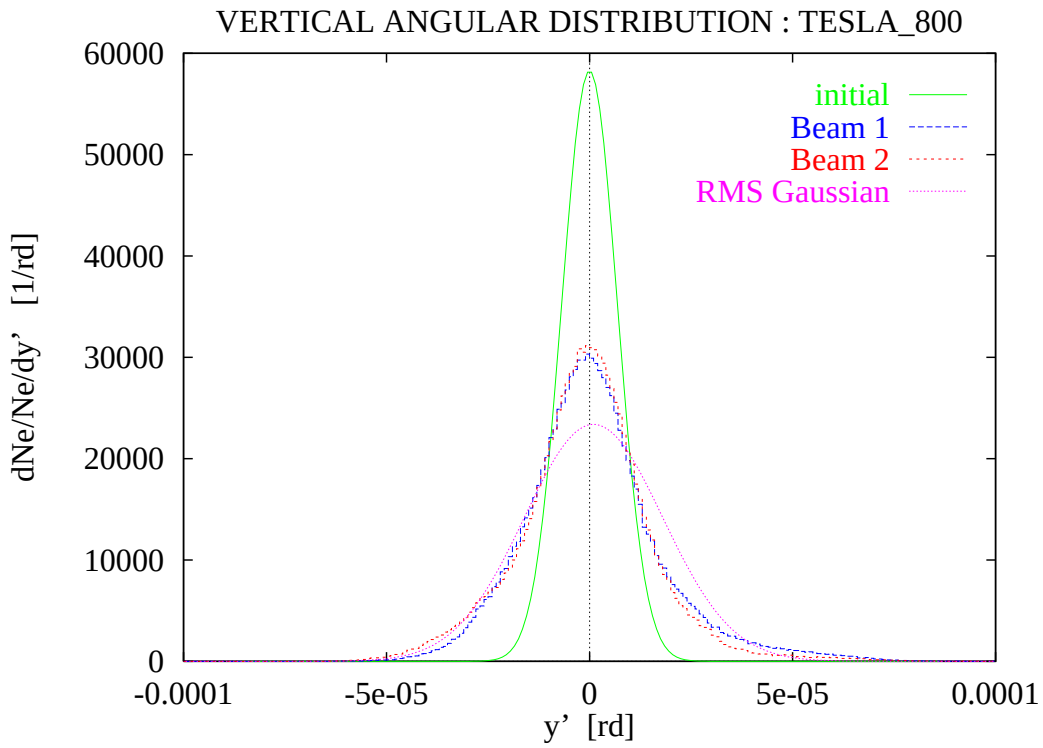

Figure 6: Spent beam angular distribution in the vertical plane for 800 GeV c.m. energy.

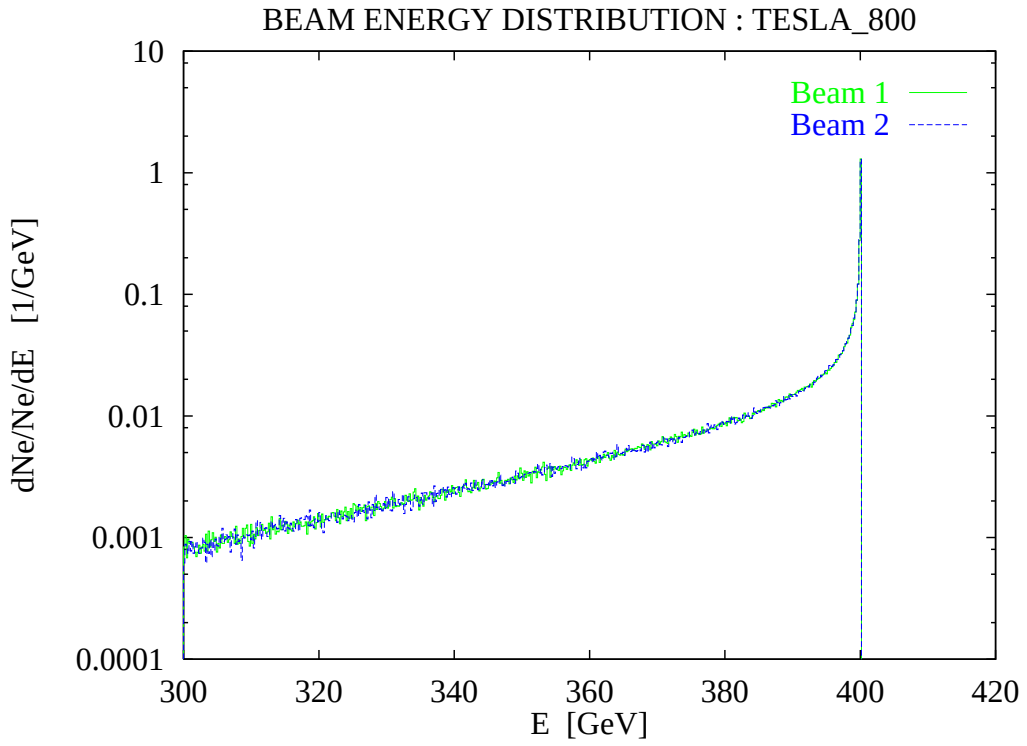

Figure 7: Spent beam energy distribution for 800 GeV c.m. energy.

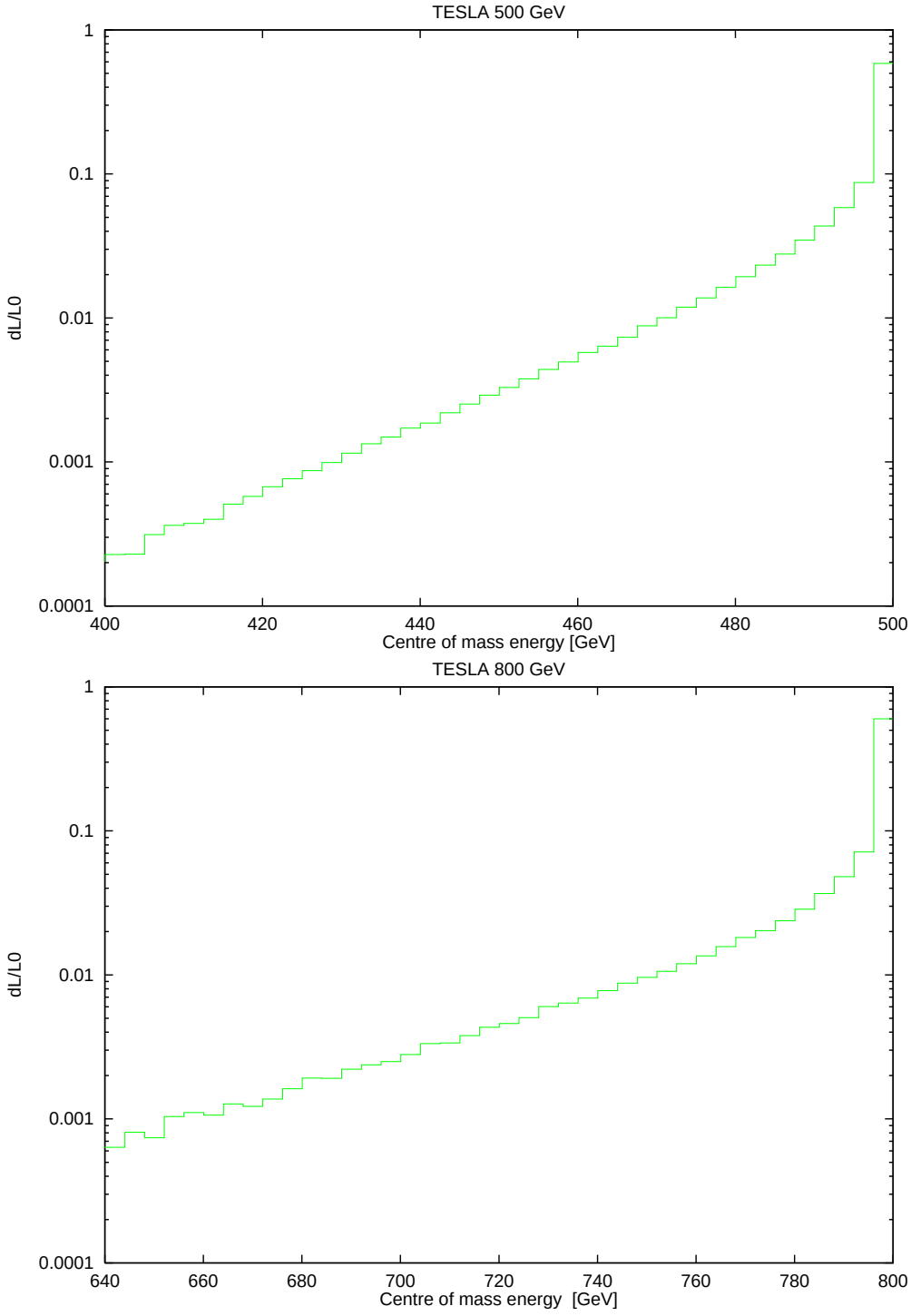

Figure 8: Luminosity spectra for 500 GeV (top) and 800 GeV (bottom) centre of mass energy

Center of mass energy [GeV]	$\sqrt{s} = 2E_0$	500	800
Luminosity per crossing [10^{30} cm^{-2}]	$\overline{\mathcal{L}}$	2.4	3.0
Upsilon parameter	Υ	0.06	0.09
Average energy loss [%]	δ_B	3.2	4.3
Spent beam power [MW]	-	11	17
Beamstrahlung Photons			
Number of photons/electron	n_γ	1.6	1.5
Beamstrahlung photon power [kW]	P_γ	360	760
Beamstrahlung photon divergences [μrad]	Θ_x^γ, Θ_y^γ	151 , 35	94 , 21
e^+e^- pairs (both sides)			
Number of particles	N_P	129 000	153 000
Average particle energy [GeV]	$\langle E_P \rangle$	2.8	5.3
# particles on LUMON1 per bunch crossing	-	36 000	36 000
Average energy on pair LUMON1 [GeV]	-	1.5	1.7
Radiative Bhabhas (both sides)			
# particles on LUMON2 per side per bunch crossing	-	1150	1700
Average energy on LUMON2 [GeV]	-	36	57

Table 3: Background parameters for head-on collisions.

positron beams is described in Ref.[3].

2. pair creation : e^+ and e^- pair particles dominate the spectrum below 20 GeV. Their profile density along the first 2.4 m of free space after the IP is plotted in Fig.10 showing their impact on a luminosity monitor (LUMON1) located at $s = 2$ m and with an aperture radius of 12 mm (see Fig.11). Their rate is so large that they can be used to monitor *relative* variations of the luminosity on a bunch to bunch basis for machine tuning purpose.

3. (beam-beam) *bremsstrahlung* : this incoherent process creates same sign low energy e^+or e^-particles, called radiative Bhabhas, moving along with the beams. While the bremsstrahlung photons escape through the beam pipe at very low angles, the radiative Bhabhas in the intermediate energy range around 40-50 GeV can be collected after the doublet. Their rate on a luminosity monitor (LUMON2) at $s = 8.5$ m and 24 mm radius, provides a signal proportional to luminosity which, although less powerful than the pair signal, can also be used for machine tuning[2].

In addition to this charged particle background, beamstrahlung photons carrying 3-4% of the beam power are emitted in a narrow forward cone of less than ± 0.15 mrad opening angle. Their angular and energy distributions are plotted in Figs.12-15 for 500 GeV c.m. energy, and in Figs.16-19 for 800 GeV c.m. energy

3.2 Background extraction

The extraction and disposal of these background particles needs special attention since, with the zero crossing-angle geometry, they are travelling backward along the opposite final focus beam line, depicted in Fig.20. Due to their low energy, the pair and radiative Bhabha particles (below 100 GeV) are overfocussed by the final doublet and stopped within the first 10 m of the outgoing beam line. Their average power deposition, shown in Fig.21 for both c.m. energies, does not exceed the 3 W/m limit allowed by the cooling of the superconducting doublet [5] ranging from $s = 3$ m to $s = 6.7$ m (see Fig.11).

In contrast, the safe extraction of the very high beamstrahlung power requires dedicated collimators to intercept tolerable fractions of this power. Fortunately, this fraction drops very fast with the solid-angle span by circular collimators as shown by Figs.15,19. The present layout uses two circular collimators located at $s = 130$ m and $s = 240$ m. The average power intercepted by these collimators as well as by closer elements in the beam lines is given Fig.20. The power, about 40 kW, which passes through the aperture of the second collimator is dumped in a solid beam dump located directly after the first C-dipole of the chromatic correction section.

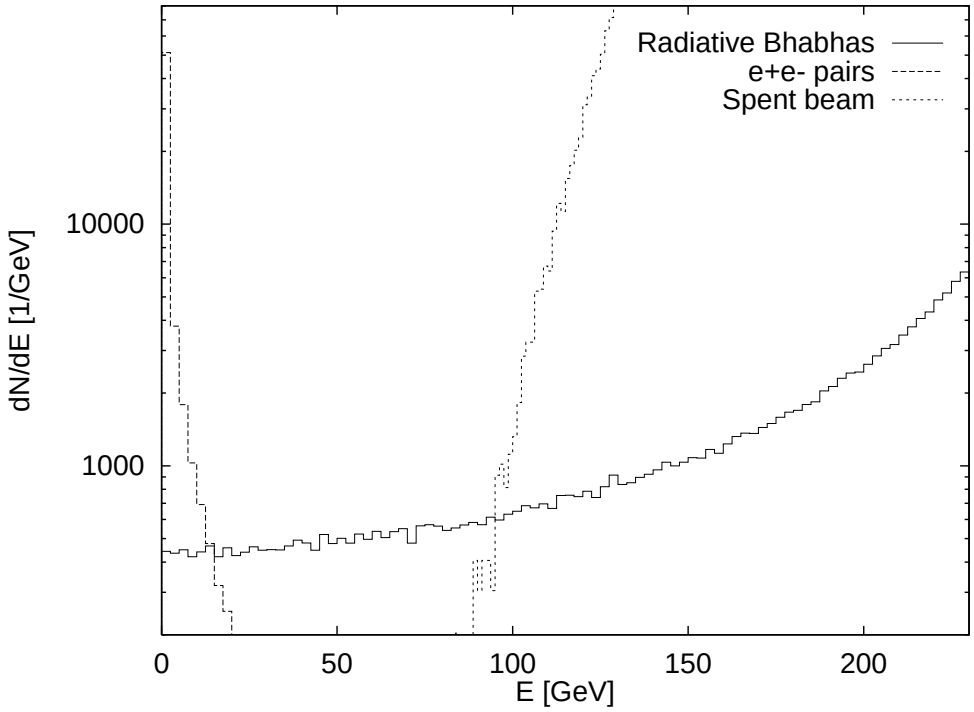

Figure 9: Energy spectrum of charged particle backgrounds for 500 GeV c.m. energy.

4 Beam-beam deflections

Beam-beam deflection scans are an essential tool to tune e^+e^- colliders. This will be also true for TESLA for tuning the horizontal parameters since, as shown by Fig.22, the beam-beam deflection curve follows very closely the analytical prediction for rigid bunches. Therefore, the measurement of the beam-beam deflections will allow an accurate measurement of the quadratic average $\Sigma_x = \sqrt{(\sigma_x^{*-})^2 + (\sigma_x^{*+})^2}$of the electron and positron horizontal beam sizes, and also of the beam relative horizontal offset. The smooth dependence of the luminosity on the relative horizontal offset is shown in Fig.23. and that of the beam relative energy loss in Fig.24.

Due to the large vertical disruption parameter D_y, the same is not true in the vertical plane: the vertical beam-beam deflection is very different from the analytic prediction for rigid bunch, as shown by Fig.25. Moreover it is also weakly dependent on the vertical beam size itself which precludes using this method to tune the quadratically averaged spot sizes Σ_y. Fortunately, as discussed above, the luminosity can be directly monitored which is usually faster and more accurate than relying on beam-beam deflection scans. As far as the fast IP orbit feedback system is concerned, the vertical beam-beam deflections are still large enough to provide a powerful signal to tune out the beam relative offset. Also related to the large vertical disruption, the luminosity decays very rapidly with vertical offsets: Fig.26 shows that the luminosity is 5 times more sentitive to small offset errors than in the case of rigid bunches (zero disruption parameter). Finally, contrary to the horizontal case, the beam energy loss increases for small vertical offsets, as shown by Fig.27, and reaches a maximum of about 4.6% at about 3-σ_y relative offset.

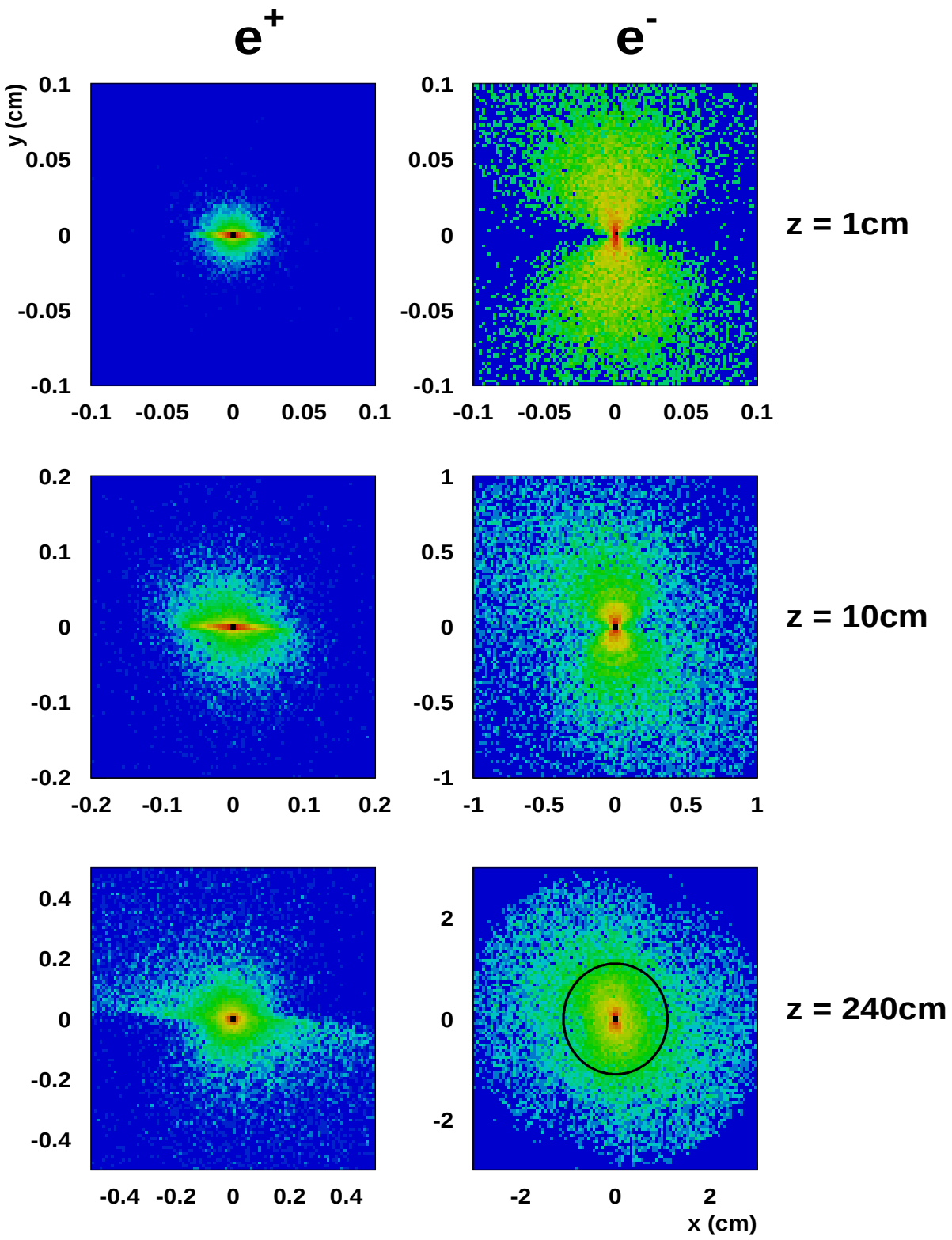

Figure 10: Transverse profiles [4] of the e^+ and e^- pair particles (500 GeV c.m. energy) along the IP drift space up to the forward mask at $s = 2 - 2.4$ m. The aperture ($r = 12$ mm) of the mask is drawn on the lower plot. Particles outside of this aperture are collected and used for monitoring the luminosity.

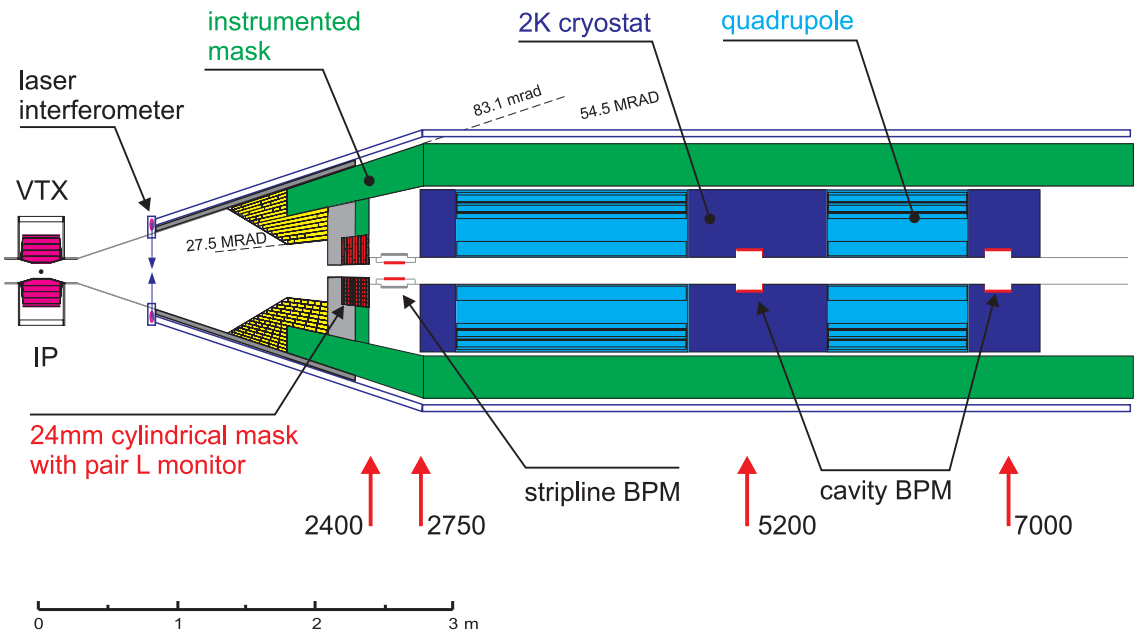

Figure 11: TESLA interaction region with detector mask and superconducting doublet.

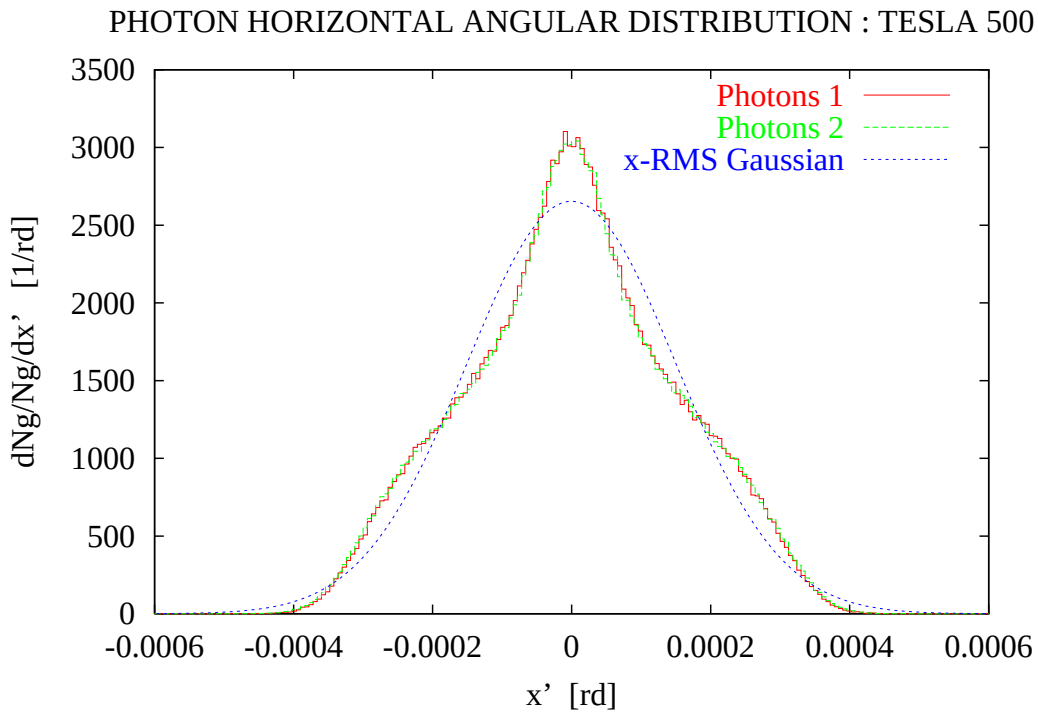

Figure 12: Beamstrahlung photon angular distribution in the horizontal plane for 500 GeV c.m. energy.

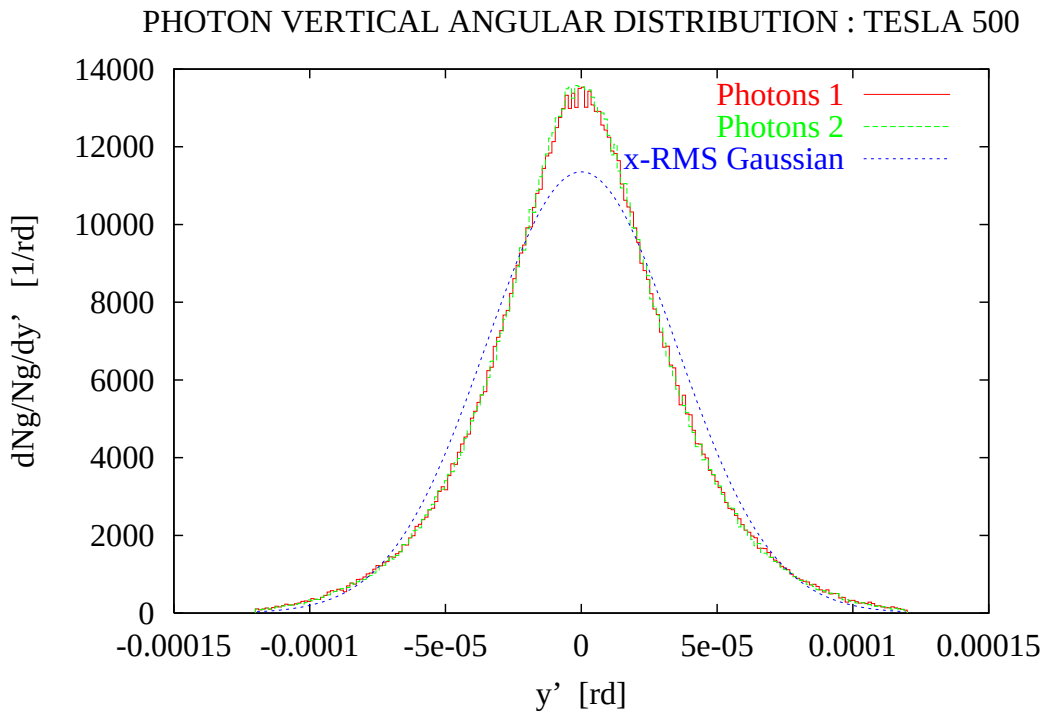

Figure 13: Beamstrahlung photon angular distribution in the vertical plane for 500 GeV c.m. energy.

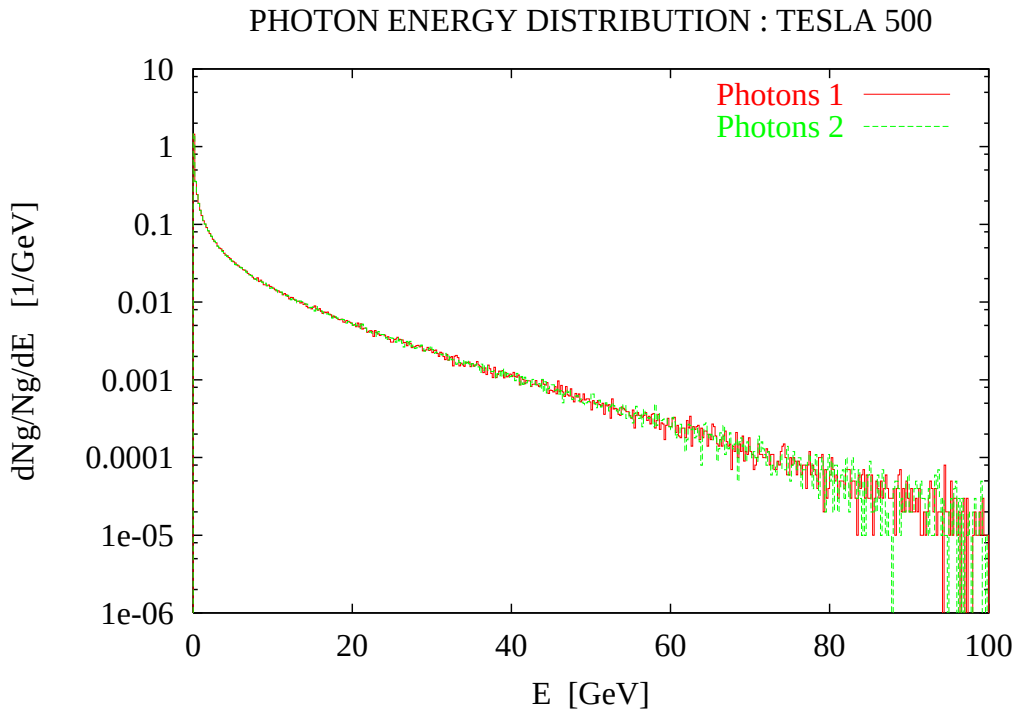

Figure 14: Beamstrahlung photon energy distribution for 500 GeV c.m. energy.

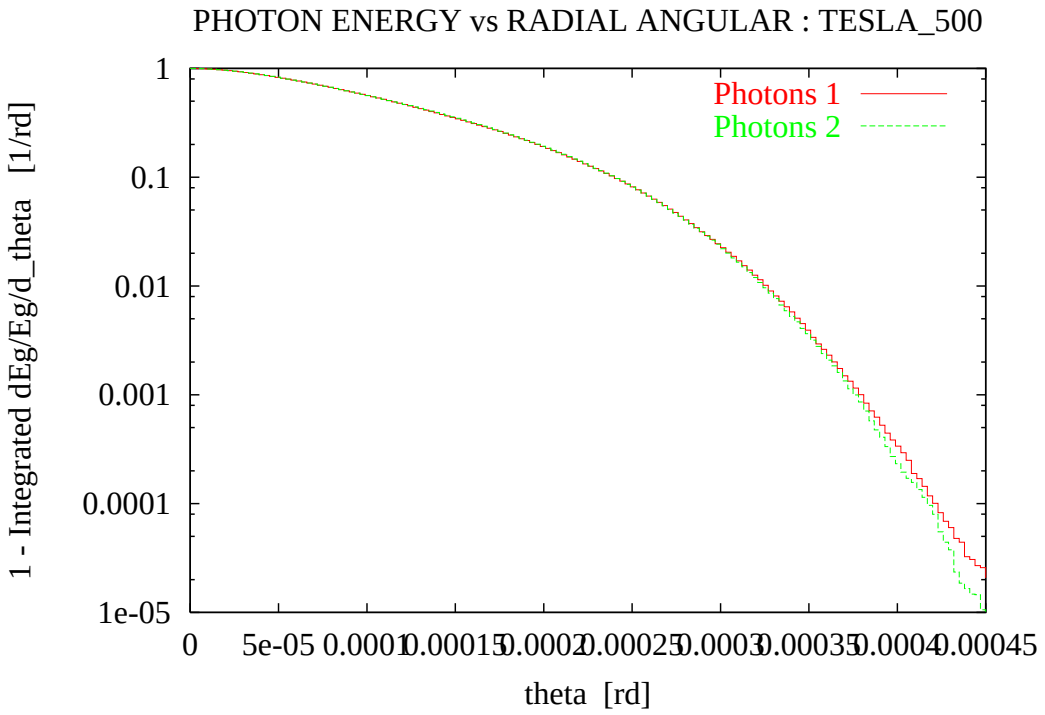

Figure 15: Fraction of beamstrahlung photon energy outside of a cone of angle θ around the beam axis, for 500 GeV c.m. energy.

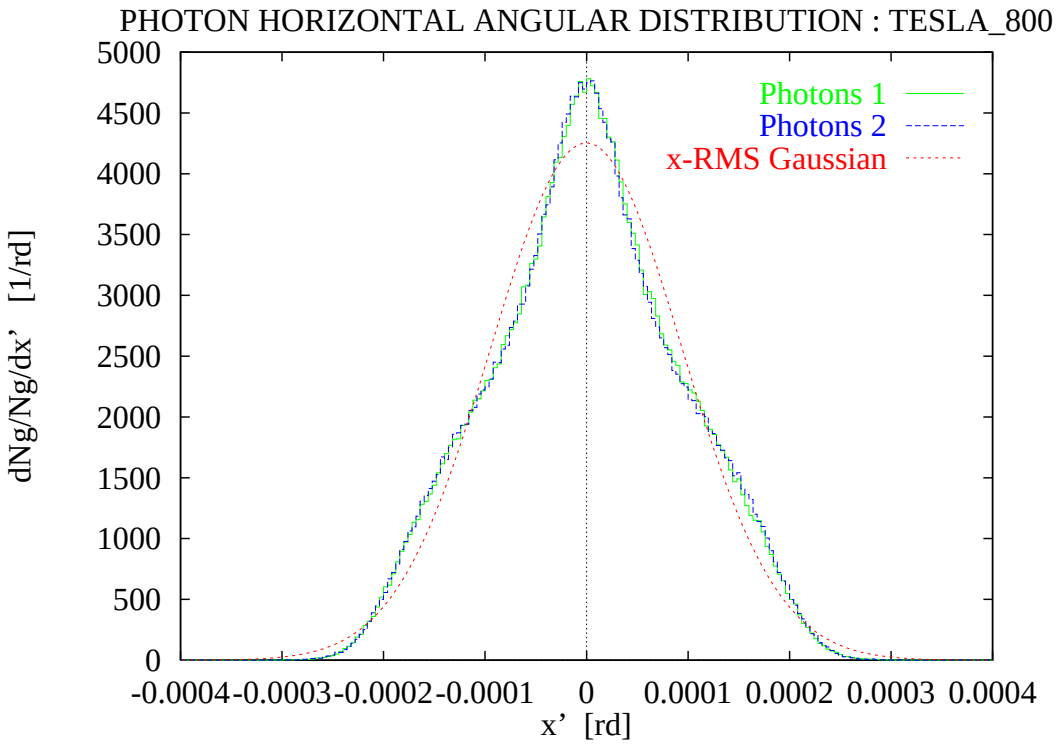

Figure 16: Beamstrahlung photon angular distribution in the horizontal plane for 800 GeV c.m. energy.

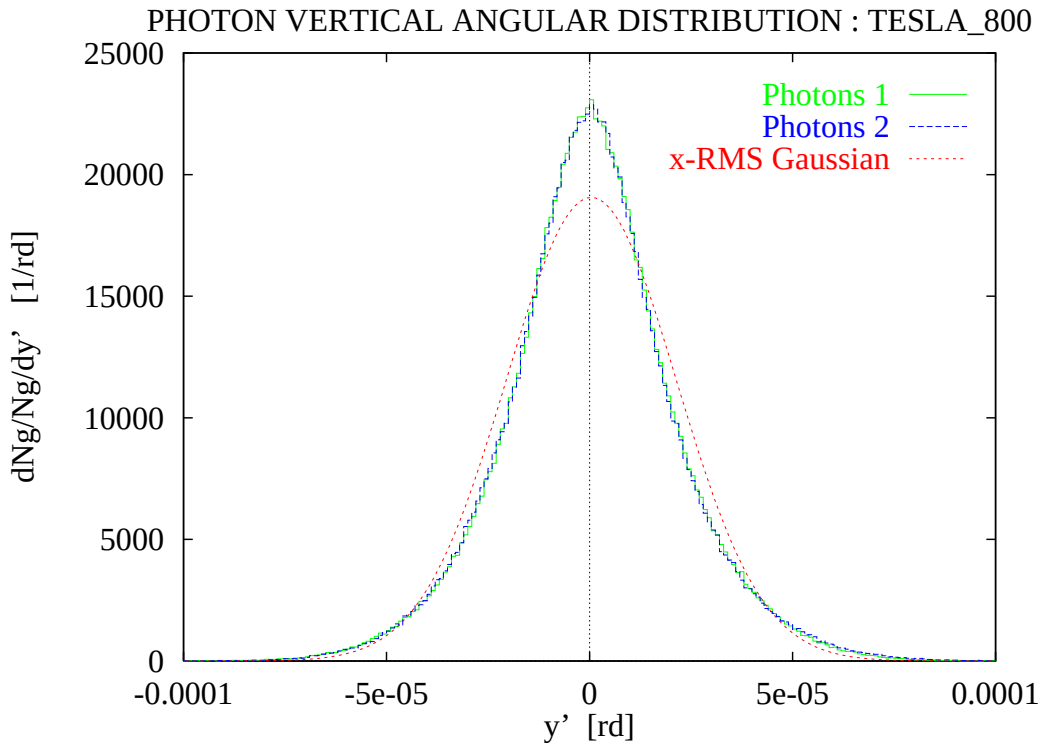

Figure 17: Beamstrahlung photon angular distribution in the vertical plane for 800 GeV c.m. energy.

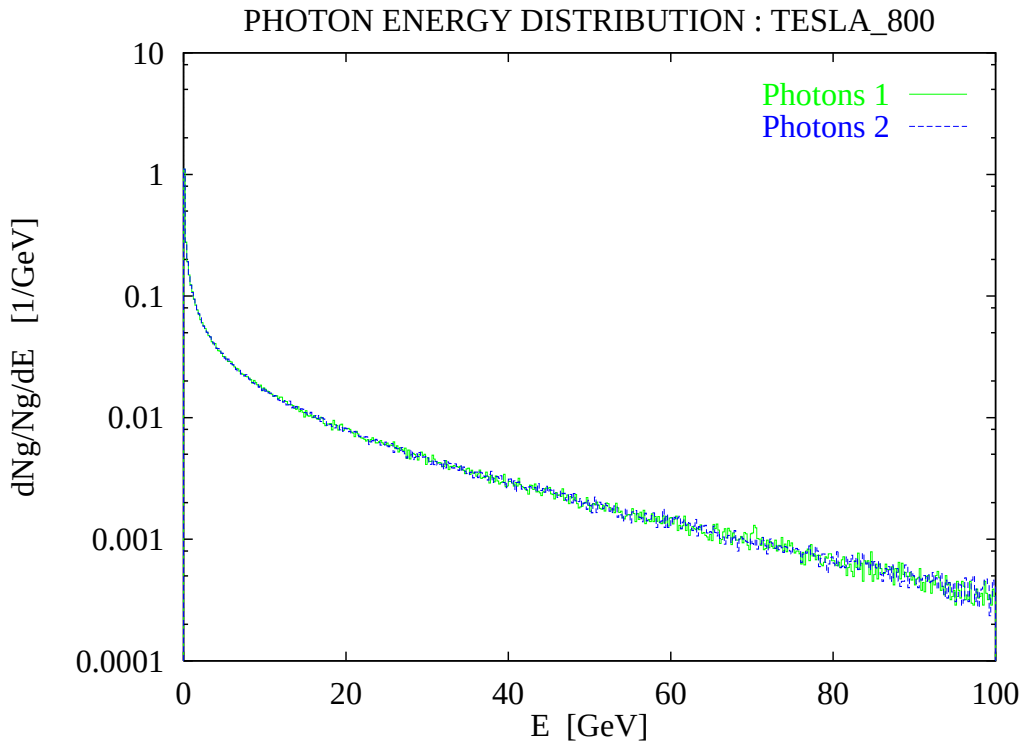

Figure 18: Beamstrahlung photon energy distribution for 800 GeV c.m. energy.

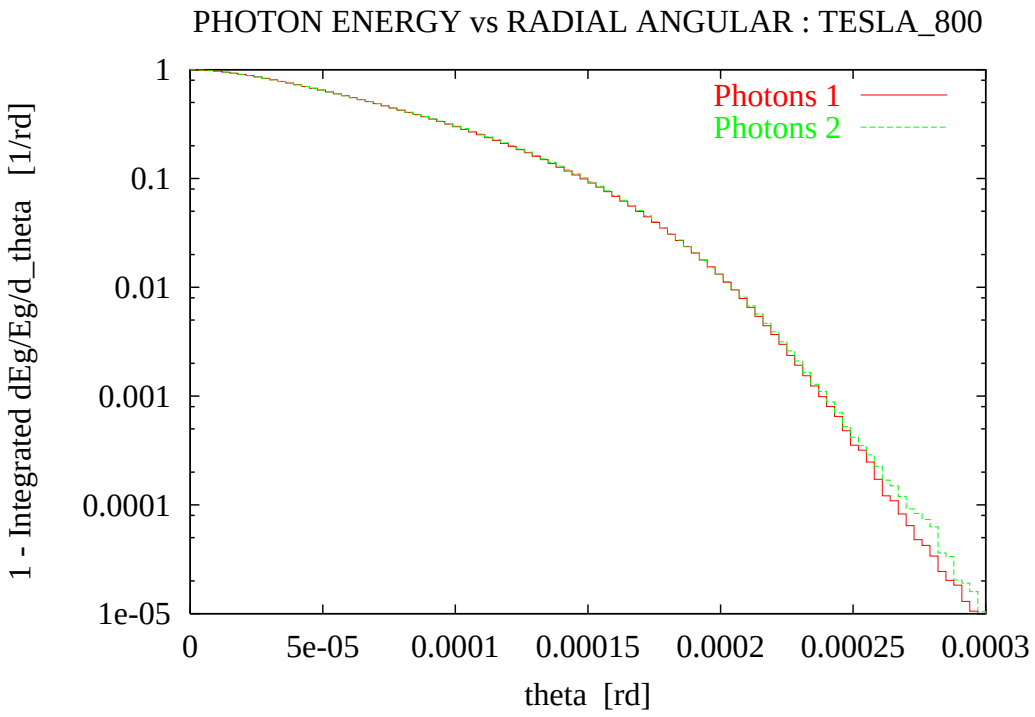

Figure 19: Fraction of beamstrahlung photon energy outside of a cone of angle θ around the beam axis, for 800 GeV c.m. energy.

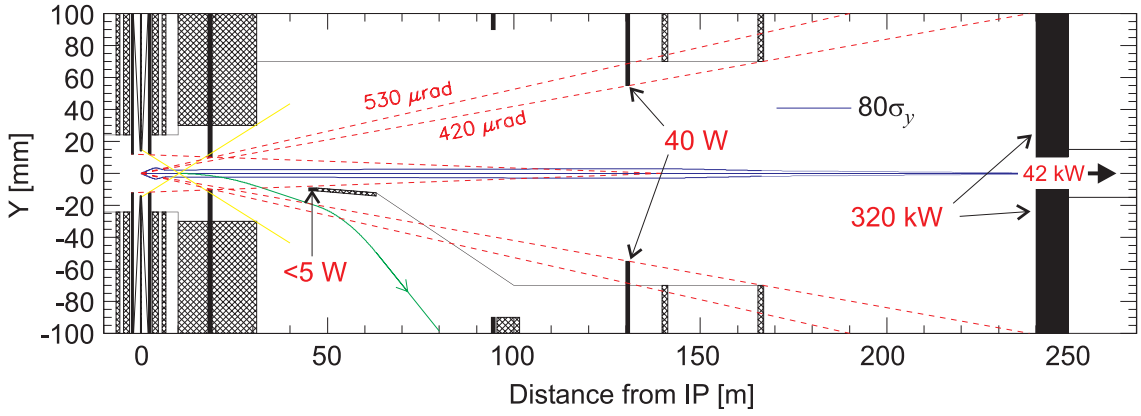

Figure 20: Final focus and main beam extraction lines (the IP is at $s = 0$ m). The beamstrahlung average power levels (indicated in red) are for 500 GeV c.m. energy.

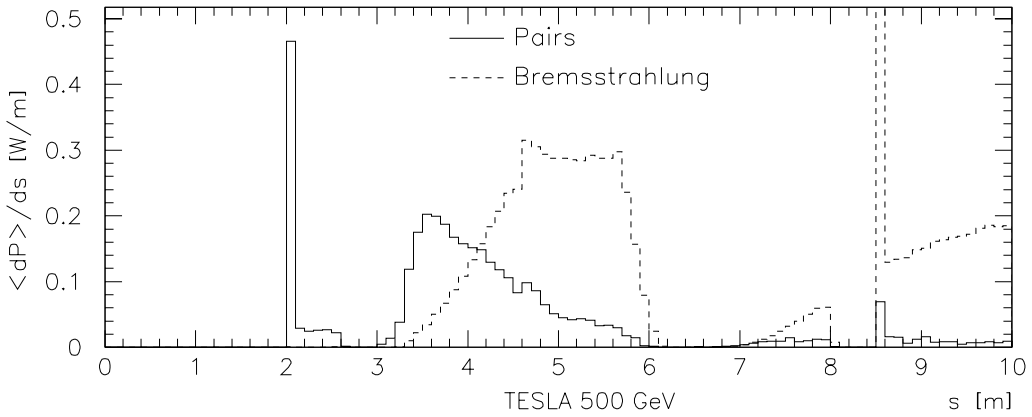

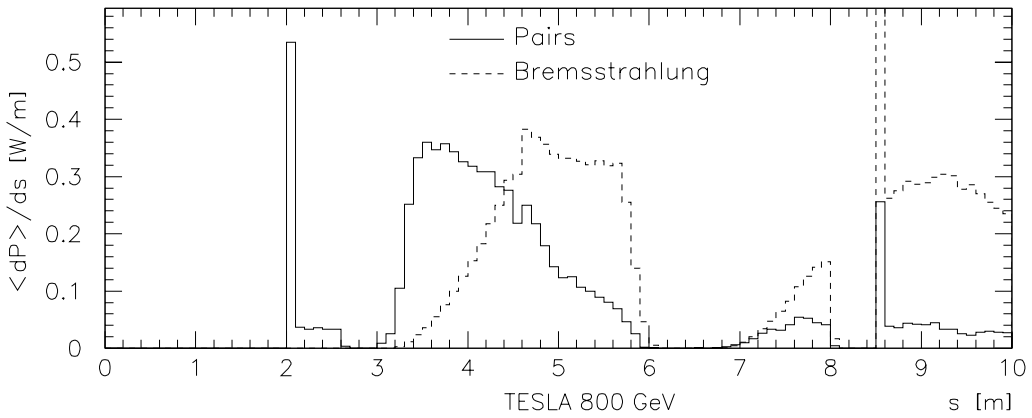

Figure 21: Average power deposition by pairs and radiative Bhabhas.

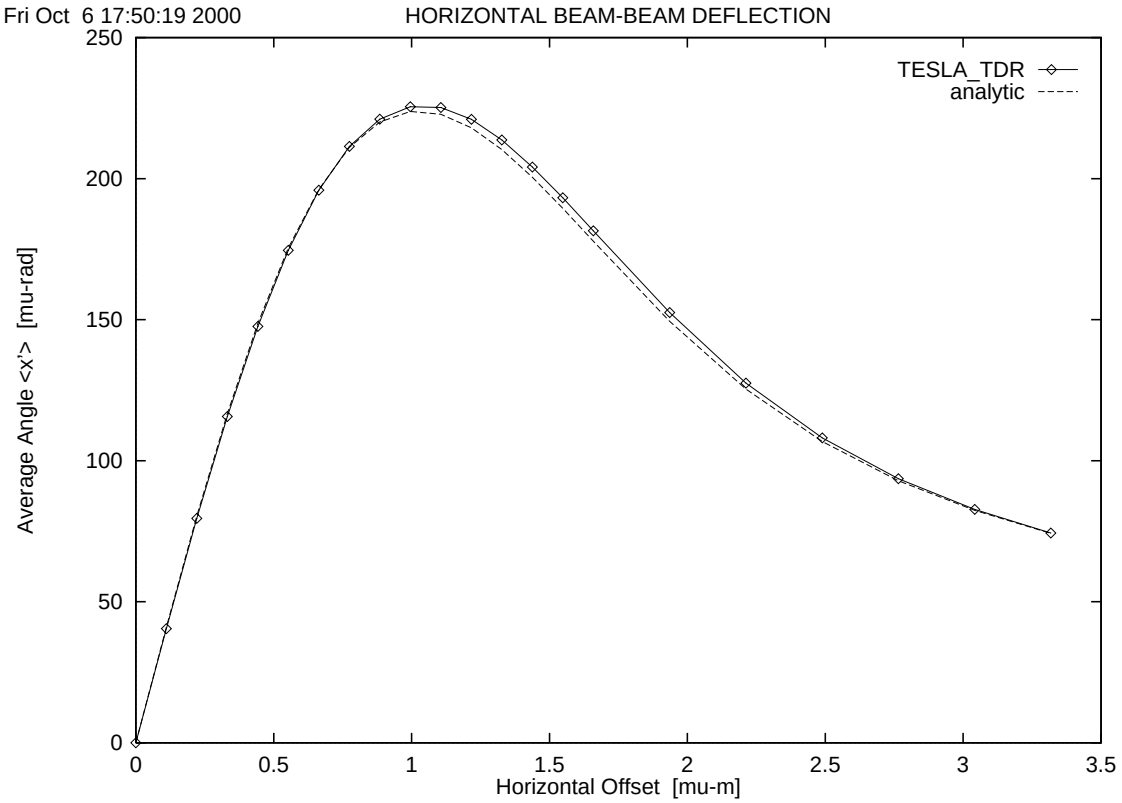

Figure 22: Horizontal beam-beam deflection for 500 GeV c.m. energy. The dashed curve is the analytic prediction for rigid bunches.

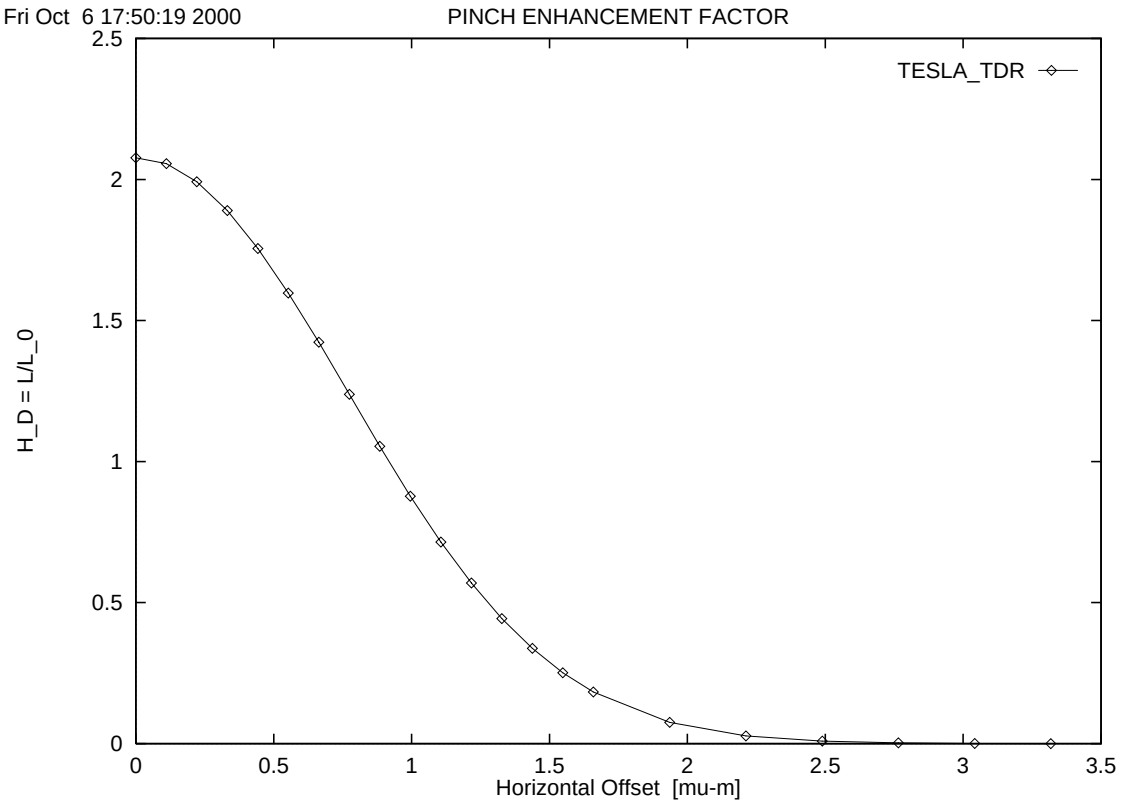

Figure 23: Luminosity enhancement factor versus beam relative horizontal offset for 500 GeV c.m. energy.

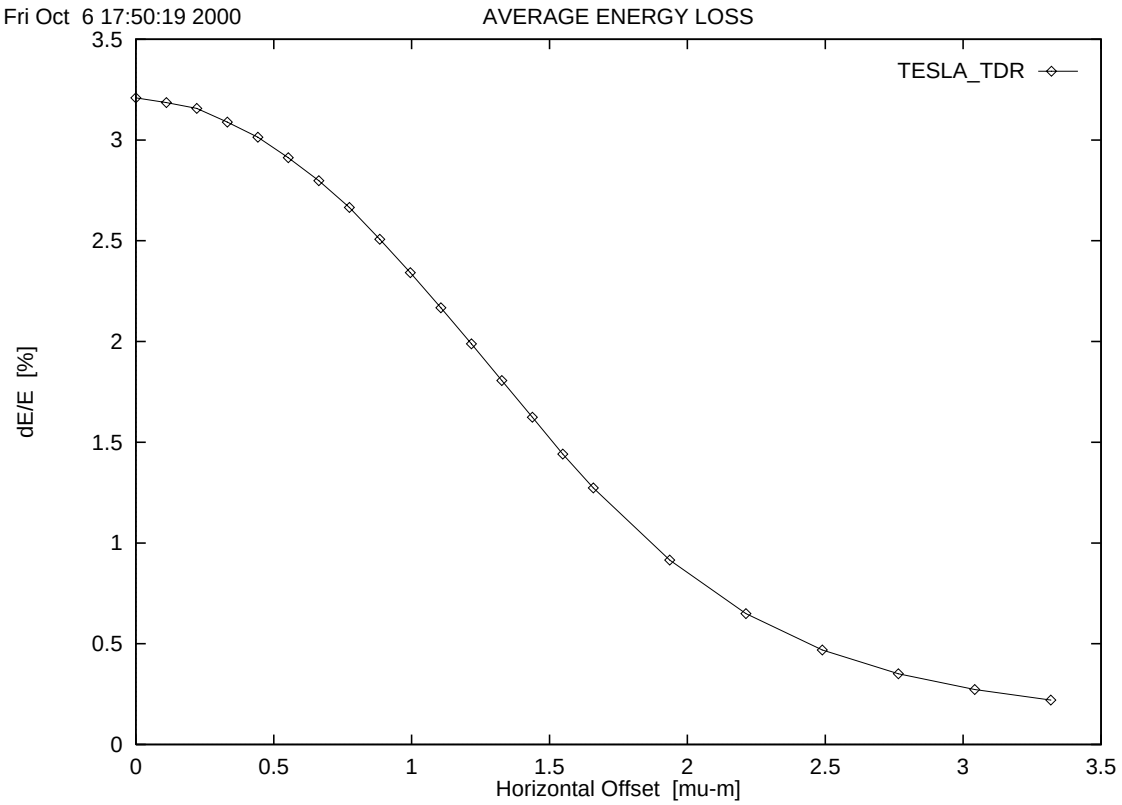

Figure 24: Relative energy loss versus beam relative horizontal offset for 500 GeV c.m. energy.

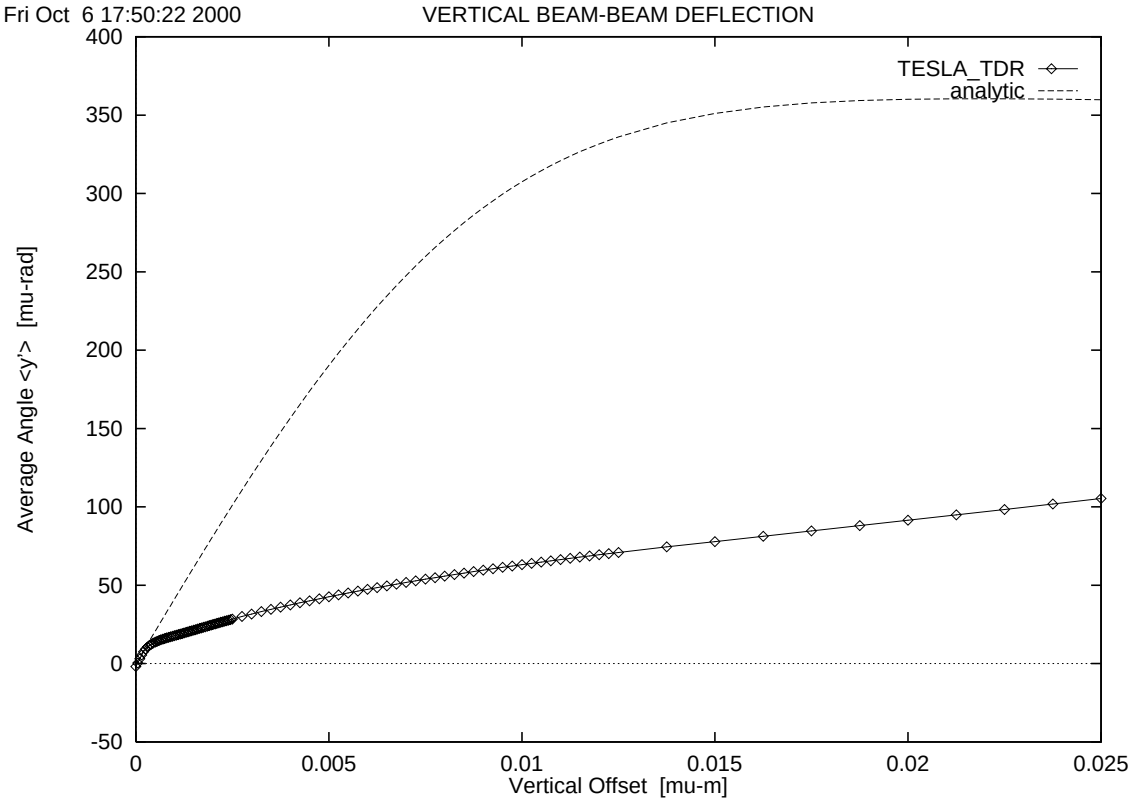

Figure 25: Vertical beam-beam deflection for 500 GeV c.m. energy. The dashed curve is the analytic prediction for rigid bunches.

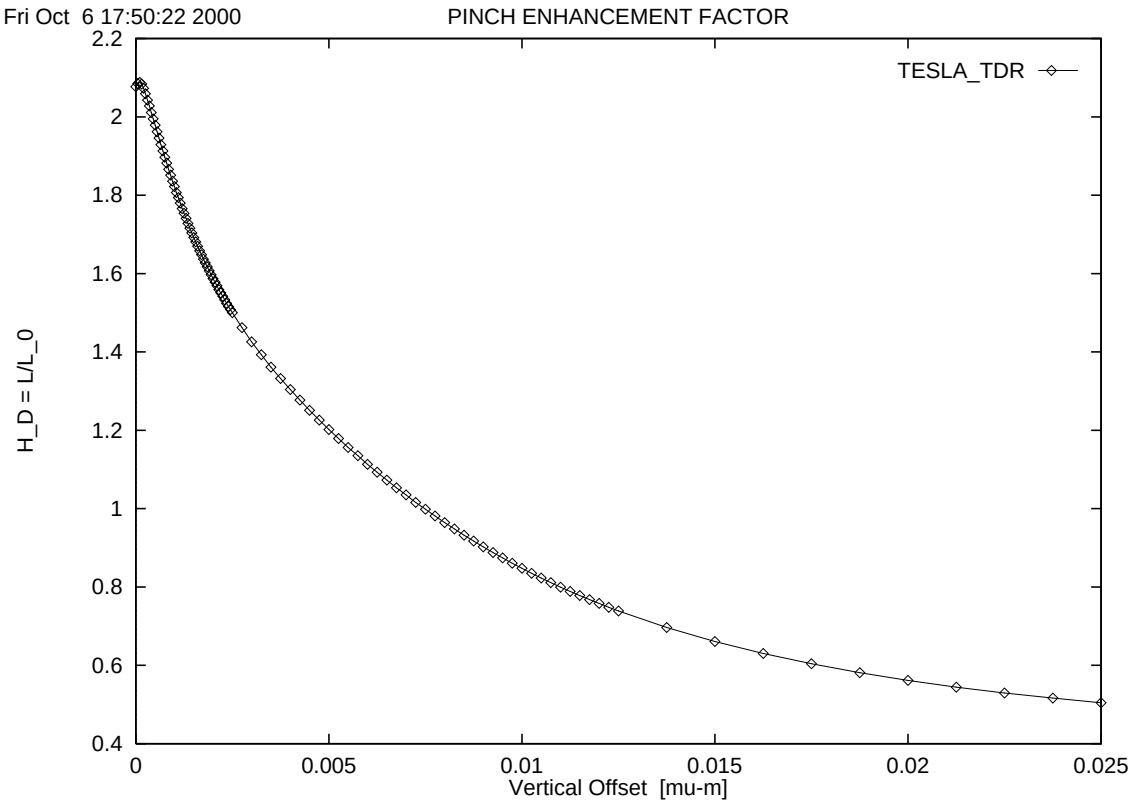

Figure 26: Luminosity enhancement factor versus beam relative vertical offset for 500 GeV c.m. energy.

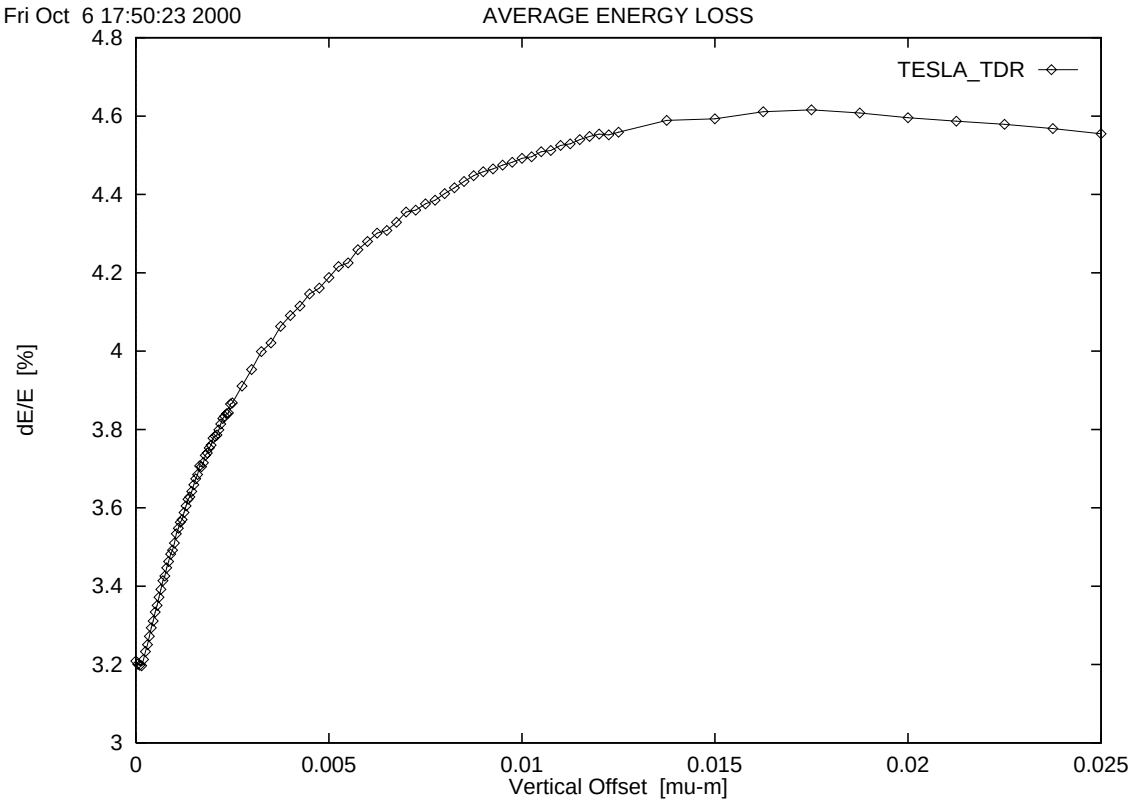

Figure 27: Relative energy loss versus beam relative vertical offset for 500 GeV c.m. energy.

The luminosity loss is even aggravated when considering the effect of small vertical angle errors at the IP : as shown by Fig.28 the luminosity is 10 times more sensitive to angle errors than in the case of rigid bunches. The beam energy loss also increases steadily to 4.6% for angle errors up to 20 mrad, as shown by Fig.29.

Although not discussed it here, the same conclusions apply for the beam-beam deflections at 800 GeV c.m. energy.

5 Improving the vertical beam-beam stability

The strong effect of global vertical IP orbit errors is corrected within a small fraction of the TESLA bunch train by the fast IP feedback systems which include both IP offset and IP angle corrections. The resulting luminosity loss is kept within 10% even for large offset and angle errors at the head of the bunch trains.

It has however a less direct but detrimental impact on the luminosity : bunch internal deformations in the vertical phase space (y, y') such as induced by linac single-bunch wakefields, the so-called "banana effect", induce an additional and sizeable luminosity loss when transported at the IP. These deformations are described by vertical translations $\langle y \rangle (z)$ and $\langle y' \rangle (z)$ of the beam centroids along the bunch, proportional to the wake potentials. They cannot be corrected by orbit and angle global corrections which cancel only the average errors. If sufficiently stable in time, they can be compensated by a different optimization of the collision parameters leading to an almost perfect recovery of the luminosity. The impact of this beam-beam instability is discussed in more details in Ref.[7].

It is worth investigating how to improve the vertical beam-beam stability of the TESLA collisions. Decreasing the bunch length is an obvious way to reduce the disruption parameter in proportion. Fig.30 compares the decay of the luminosity with IP offset and angle errors for the nominal bunch length $\sigma_z = 300\,\mu$m and the case where $\sigma_z = 200\,\mu$m. The improvement in luminosity stability is quite important, especially for the angle errors. The price to pay is in the increased performance of the bunch compressor system, the larger energy spread at linac injection and, also

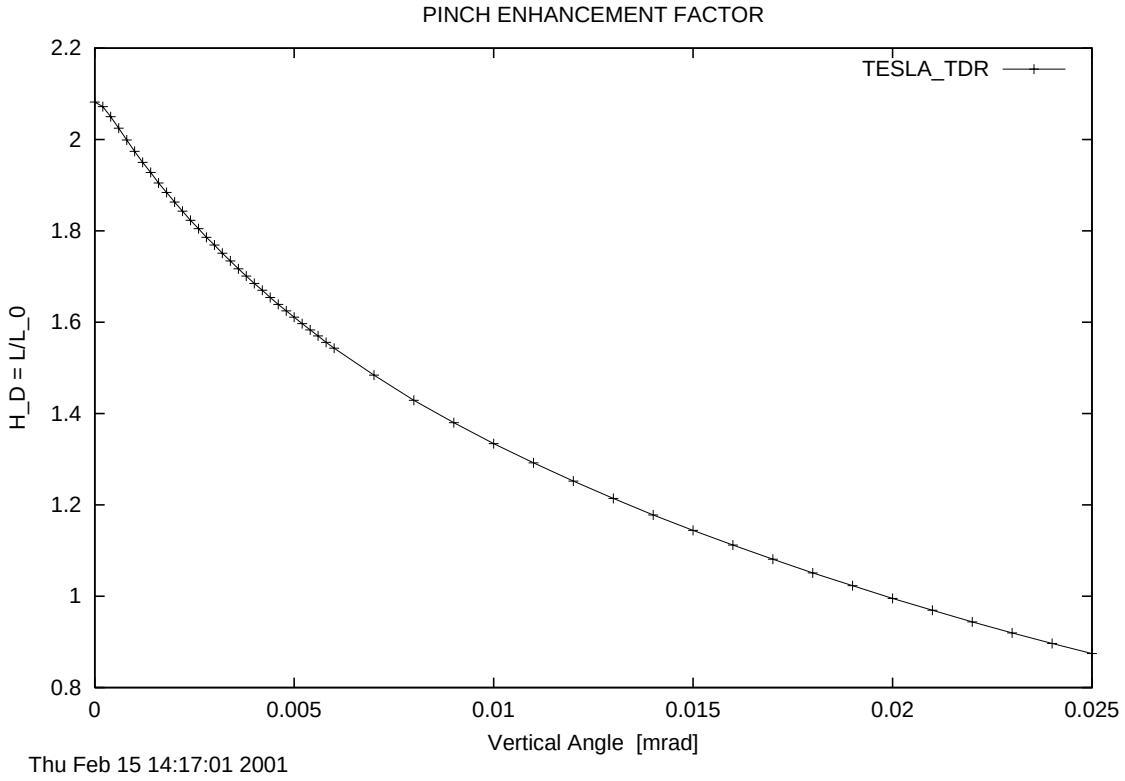

Figure 28: Luminosity enhancement factor versus beam relative vertical angle for 500 GeV c.m. energy.

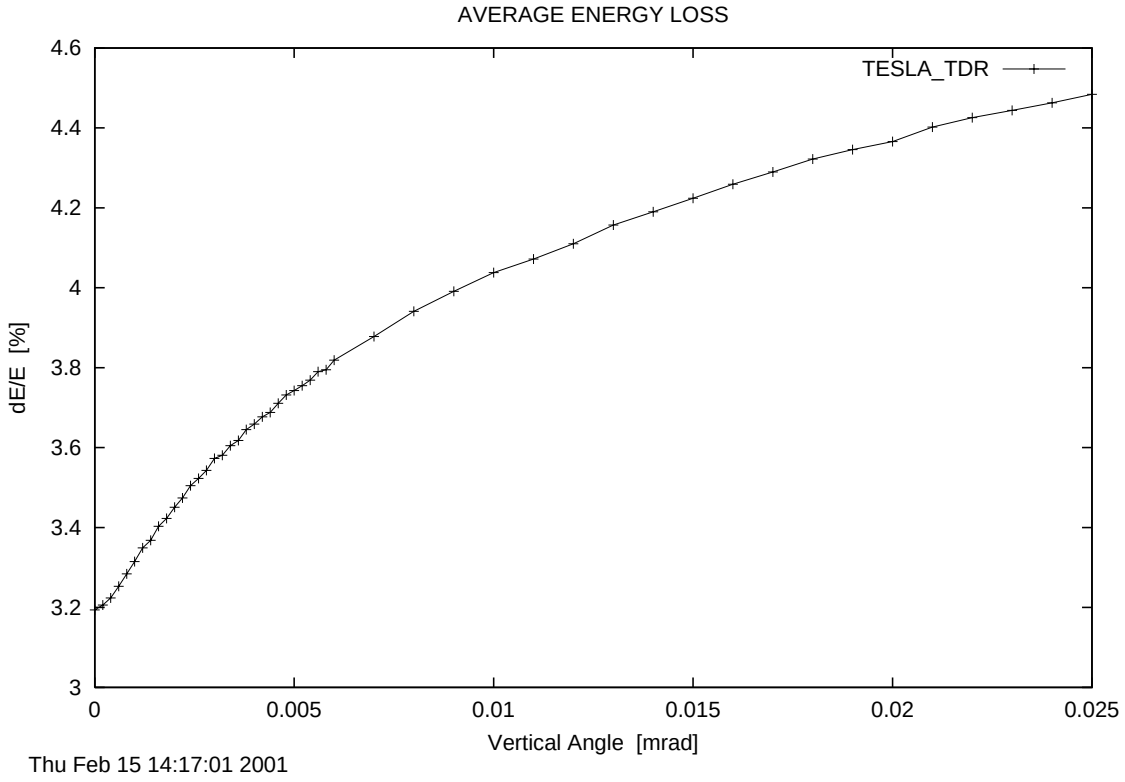

Figure 29: Relative energy loss versus beam relative vertical angle for 500 GeV c.m. energy.

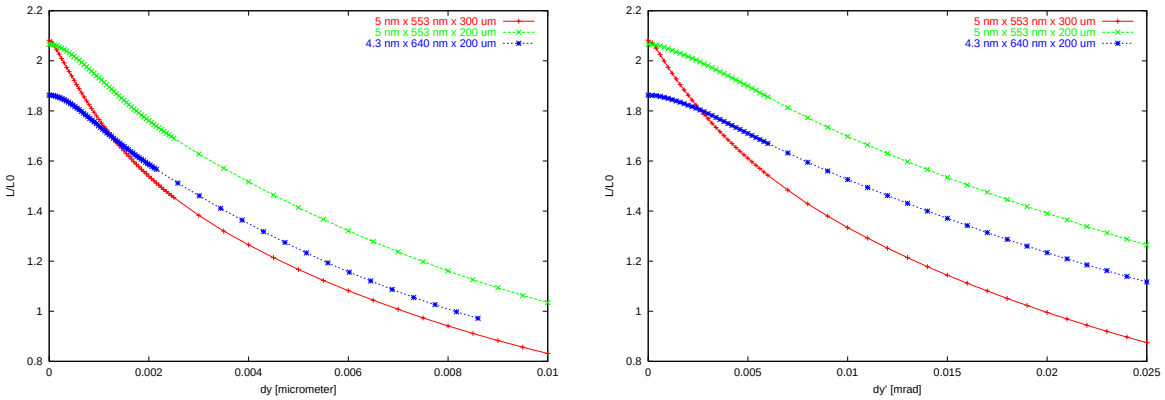

Figure 30: Comparison of the decay of the luminosity with vertical IP offset (left) and vertical IP angle (right) for the nominal TESLA parameters $\sigma_z = 300\,\mu$m and two other sets of parameters with a reduced bunch length $\sigma_z = 200\,\mu$m and a smaller vertical disruption parameter.

the larger beamstrahlung energy spread, 4.1% instead of 3.2%. The beamstrahlung energy spread can be recovered by colliding beams with a larger aspect ratio. Fig.30 also compares the luminosity for 640nm×4.2nm beam spot sizes at the IP obtained by reducing β_y^* from 400 μm to 300 μm and keeping the same transverse cross-section as the nominal one. As expected the pinch enhancement factor is smaller for the flatter beam but the energy loss is reduced to 2.4% and the luminosity decays much slower. The price is then in the more difficult correction of the vertical chromaticity.

References

[1] D. Schulte, *Beam-beam Simulations with GUINEA_PIG*, CERN-PS-99-14, CERN-CLIC-Note-387, 1999.

[2] O. Napoly and D. Schulte, *Luminosity Monitor Studies for TESLA*, DESY TESLA-97-17 and Saclay preprint CEA/DAPNIA/SEA-97-14 , 1997 and, CEA/DAPNIA/SEA-98-51.

[3] E. Merker, I. Yazynin, O. Napoly, R. Brinkmann and N. Walker, *The TESLA High-Power Extraction Line*, TESLA-2001-19, 2001.

[4] K. Büßer, *Mask Design and Background Studies for TESLA,* Proceedings of the LCWS2000 workshop, October 24-28, 2000, Fermilab, Batavia, USA.

[5] A. Devred et al., *Conceptual Design for the Final Focus Quadrupole Magnets for TESLA*, DESY TESLA-2001-17, 2001.

[6] I. Reyzl, *Stabilisation of Beam Interaction at the TESLA Linear Collider*, Proc. 7th EPAC, Vienna 2000, p.315.

[7] R. Brinkmann, O. Napoly and D. Schulte, *Beam-beam Instability Driven by Wakefield Effects in Large Disruption Linear Colliders*, DESY TESLA-2001-16, 2001